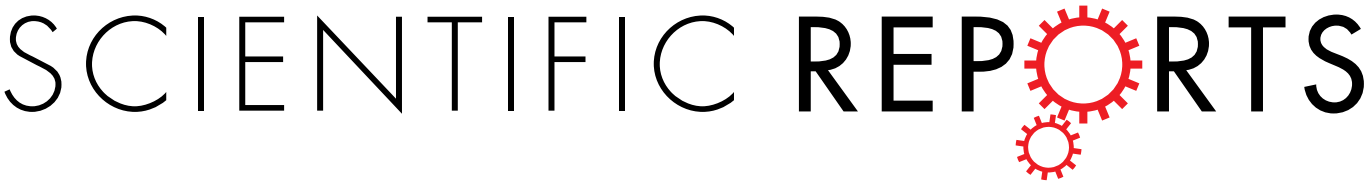

OPEN

Universal classification of twisted, strained and sheared graphene moiré superlattices

Received: 29 December 2015
Accepted: 12 April 2016
Published: 16 May 2016

A. Artaud[1,2,3], L. Magaud[1,2], T. Le Quang[1,3], V. Guisset[1,2], P. David[1,2], C. Chapelier[1,3] & J. Coraux[1,2]

Moiré superlattices in graphene supported on various substrates have opened a new avenue to engineer graphene's electronic properties. Yet, the exact crystallographic structure on which their band structure depends remains highly debated. In this scanning tunneling microscopy and density functional theory study, we have analysed graphene samples grown on multilayer graphene prepared onto SiC and on the close-packed surfaces of Re and Ir with ultra-high precision. We resolve small-angle twists and shears in graphene, and identify large unit cells comprising more than 1,000 carbon atoms and exhibiting non-trivial nanopatterns for moiré superlattices, which are commensurate to the graphene lattice. Finally, a general formalism applicable to any hexagonal moiré is presented to classify all reported structures.

Graphene (gr) is a two-dimensional crystal with honeycomb structure, whose peculiar electronic properties have raised considerable interest in the past few years. Indeed, its electronic bands cross at the K and K' corners of the Brillouin zone, giving rise to a linear energy dispersion of its quasiparticles close to the Fermi level[1]. Moreover, the bipartite nature of graphene's lattice, with two triangular carbon sub-lattices (A and B), confers unique properties to these quasiparticles. By analogy to quantum electrodynamics[2], a sublattice-related quantum number, so-called pseudo-spin, equivalent to the spin of Dirac fermions is defined[3]. For these reasons, the conical electronic bands around the K and K' points of the Brillouin zone are called Dirac cones.

Such exotic electronic properties are predicted for pristine graphene, but are altered when graphene is supported by a substrate. Indeed, due to the structural mismatch between graphene and its support, graphene has periodically varying stacking configurations with its substrate[4–9]. This effect modulates the graphene-substrate interaction and distance[10–14], over a so-called moiré periodicity, which can range from ~1 to ~15 nm. Depending on the interaction between graphene and the substrate, the moiré can have a dramatic impact on graphene's properties. Some substrates impose only a weak interaction dominated by van der Waals forces, which is the case for graphene on hexagonal boron nitride[15] or multilayer graphene on the carbon face of SiC[16]. In this case, the graphene-substrate distance is about 3.4 Å (refs 16,17), very close to the value 3.3539 Å of highly oriented pyrolytic graphite (HOPG)[18], and graphene's electronic properties are mostly preserved[17,19]. In these systems, the moiré acts as a smooth superpotential that varies slowly compared to the one associated to carbon atoms. The corresponding unit cell, which is larger than the one of pristine graphene, is associated with replica Dirac cones, reduced Fermi velocity[20–23], with either superlattice Dirac cones[21,22,24,25] or mini-gaps[20,26] at the moiré Brillouin zone boundary. Such properties make this system an ideal playground to investigate quantum phases arising in periodic two-dimensional electron gases subjected to an external magnetic field[25–27]. In bilayer graphene samples, Van Hove singularities and electron localization also emerge from the coexistence of the Dirac cones of each layer[28,29]. Overall, in low-interaction systems, tuning moiré superlattices is a mean to tailor graphene's electronic properties.

Other surfaces interact more strongly with graphene, and are prone to exchange electrons with it, establishing partially covalent bonds. Graphene-substrate bonding then implies both van der Waals forces (physisorption) and partial covalent bonding (chemisorption), and is modulated along the moiré periodicity[11,12,30–32]. Graphene is thus nanorippled, the shortest graphene-substrate distances showing tendency to covalent bonding. Nanorippling amplitudes varying from 0.03 (on Pt(111)[33]) to 1.6 Å (on Re(0001)[32]) have been reported depending on the strength of the graphene-substrate interaction[8]. Systems with strong nanorippling amplitudes usually

[1]Univ. Grenoble Alpes, F-38000 Grenoble, France. [2]CNRS, Inst NEEL, F-38000 Grenoble, France. [3]CEA, INAC-PHELIQS, F-38000 Grenoble, France. Correspondence and requests for materials should be addressed to A.A. (email: alexandre.artaud@cea.fr)

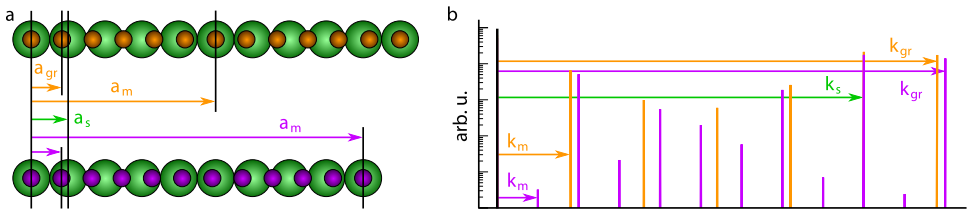

Figure 1. Moiré superlattice and beatings: (**a**) Ball model of a chain of (small) carbon atoms in graphene on top of a chain of (large) atoms from the support, both having different lattice parameters a_{gr} and a_s, whose commensurability defines a moiré superlattice with period a_m. For 6 graphene periods matching 5 support periods (orange), a single beating occurs within the moiré period, and the fast Fourier transform (FFT) reveals a fundamental harmonic defined by $k = (k_{gr} - k_s)/(6 - 5)$ (**b**). For 11 graphene periods matching 9 support periods (purple), two beatings occur within the moiré period, with similar stacking configurations at the edges and at the middle of the ball model. The corresponding FFT reveals a fundamental harmonic at $k = (k_{gr} - k_s)/(11 - 9)$ (**b**).

have valence and conduction bands without Dirac fermion character[34,35]. For all those metals, however, the moiré modulation of graphene's electronic properties goes along with a modulation of its chemical reactivity, inducing preferential sites for adsorbtion or functionalization. This makes moiré superlattices efficient to self-organize arrays of metallic clusters[36,37] and molecules[38,39]. For gr/Ir, they can in turn influence the electronic properties of graphene, for instance opening a band gap[35,40] or tuning the Fermi level and velocity[41,42].

The usual structural model used to describe moirés assumes (Fig. 1a top) that a single moiré beating occurs within a moiré period and that the graphene and moiré lattices are commensurate (integer multiples of their lattice parameters can be found which are equal). This superlattice model was for instance often used to describe gr/Ir, but eventually proved too restrictive to describe the variety of situations observed in experiments (see refs 43–48 for gr/Ir) depending on growth conditions[49] and sample history[47,50]. Accordingly more general models have been proposed. Some simply assume that the graphene and moiré lattices are incommensurate[36]. Others assume commensurability, yet without the constraint of a single moiré beating within the moiré unit cell. This situation is sketched in Fig. 1a (bottom) and accounts for experimental data obtained with gr/Ru and gr/Ir, for which four beatings were proposed in case of the zigzag rows of graphene aligning the close-packed ones of the metal[47,49,51,52] and even more in graphene whose zigzag rows are ~30° rotated[43].

There are many ways the above assumption for commensurability can be fulfilled, as can be shown by considering strains and rotation of the graphene with respect to its substrate[53]. For substrates exerting a weak bonding with graphene, rotations readily occur[43,54]. Strain, on the contrary, is more energetically costly in reason of the high mechanical stiffness of graphene[55]. It appears that strains beyond few percents are not achievable in graphene synthesized on a substrate. Formal treatments of strain so far exclusively assumed biaxial strain. One noticeable exception is the description given by Hermann[56]. This description relates geometrical transformations to a set of indices characterizing the commensurability between two triangular lattices. Among the transformation considered in Hermann's work is a shear strain, applied with a similar magnitude for the two lattices. The recently observed case of sheared graphene onto a rigid unsheared lattice[49], such as a metallic substrate whose deformations induced by graphene can be neglected, is not accounted for to our best knowledge.

Here we present the straightforward extension of Hermann's formalism to the latter case. Besides, we derive the relationships that establish the consistency between this formalism, and another one, recently presented by Zeller and Günther to describe the number of beatings a moiré can comprise[57]. Overall, with the help of geometrical transformations, we provide a fully-consistent description of the full complexity of commensurate moiré superlattices, relating the graphene, substrate, and moiré, for the general case of an arbitrary strain (including shear, uniaxial, biaxial) and of superlattices having any number of beatings. This transformation is expressed within a matrix formalism and in an extension of the so-called Wood's notation, which gives the angles formed between the unit cell vectors of graphene and the moiré as well as the ratio between these vectors' length. We use the latter notation to construct maps of the possible commensurate moiré superlattices and to revisit previously published analysis of experimental observations. We show that supported graphene is subjected to strain levels far below what is usually assumed.

We apply this description to resolve the structure of the moiré superlattices in graphene on multilayer graphene prepared on SiC, and in monolayer graphene on Re(0001) and Ir(111). For this purpose, we resort to scanning tunneling microscopy (STM) in both direct and reciprocal (Fourier) space, in the latter case achieving better than 0.1 pm precision on the lattice parameter determination, owing to distortion-less imaging with atomic resolution across several 10 nm fields of view. We find rotated and sheared moiré superlattices. Similarly to the rotation, shear appears more obviously in the moiré than in the graphene, as confirmed by our density functional theory (DFT) calculations. Some of these moirés comprise several moiré beatings in the case of metal substrates. Strikingly, commensurability between graphene and moiré superlattices provides a fine description of even very large moiré supercells, comprising above 1,000 carbon atoms.

Results

General framework. In most cases, supported graphene and its substrate do not share the same lattice parameter and/or graphene lies twisted by some angle with respect to its support. Assuming commensurability between the two lattices, a supercell can be defined which comprises the smallest integer numbers of unit cells

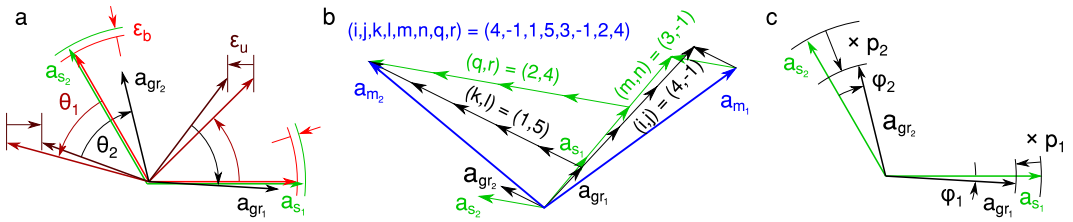

Figure 2. Structural interpretation of a moiré superlattice: (**a**) The transformation relating graphene lattice vectors ($\mathbf{a}_{\mathbf{gr}_1}$, $\mathbf{a}_{\mathbf{gr}_2}$) to those of its support ($\mathbf{a}_{\mathbf{s}_1}$, $\mathbf{a}_{\mathbf{s}_2}$) can be decomposed into four steps. (**1**) Graphene vectors are isotropically rescaled with respect to those of the support (light red). (**2**) Graphene is rotated with respect to its support (red), in order to determine the direction in which (**3**) a horizontal rescaling is applied (dark red). (**4**) A final rotation is applied (black). (**b**) The lattice vectors of the moiré superlattice decompose into both graphene and support bases, giving $(i, j, k, l, m, n, q, r) = (4, -1, 1, 5, 3, -1, 2, 4)$. (**c**) Corresponding extended Wood's notation: $(p_1\,\mathbf{R}\varphi_1 \times p_2\,\mathbf{R}\varphi_2)$, where p_1 and p_2 are scaling factors, and φ_1 and φ_2 are rotation angles.

of both graphene and the support. This supercell defines the moiré superlattice. Formally, in a one-dimensional picture, the moiré superlattice parameter a_m is an integer number times graphene's (a_{gr}) or the support's (a_s) lattice parameters: $a_m = i\,a_{gr} = m\,a_s$, with i and m two coprime integers.

Still in one dimension, the reciprocal (Fourier) space unit vectors of the moiré superlattice (k_m), of graphene (k_{gr}) and of the support (k_s) hence fulfil $i\,k_m = k_{gr}$ and $m\,k_m = k_s$. We stress that these two equations constitute the general definition of a moiré superlattice. On the contrary, the definition usually proposed in the literature, $k_m = k_{gr} - k_s$, does not require commensurability. It can be obtained in the particular case of a commensurate system, with $i - m = 1$, *i.e.* with i and m two consecutive integer numbers. This particular case is sketched in Fig. 1a (top). Figure 1b shows a different situation with $i - m = 2$. Strikingly, at first sight the two moirés in Fig. 1a are very similar. Indeed, at the middle of both linear ball models, the stacking of the carbon atoms onto the substrate ones is similar. In an analogy with optics, beatings between the two lattices seem to occur at the same location. Careful inspection however reveals that, for the $i - m = 1$ moiré (Fig. 1a top), the carbon atom sits exactly on top of the atom underneath, while for the $i - m = 2$ moiré (Fig. 1a bottom), the coincidence is only approximate. The difference is most often subtle in a scanning probe microscopy experiment[52] (similar graphene/support stackings yield similar signals), and usually overlooked, so the $i - m = 2$ is generally (erroneously) described as a $i - m = 1$ moiré. In fact it has a richer Fourier spectrum than the latter, as can be seen on Fig. 1b. The fundamental Fourier harmonic of the $i - m = 2$ moiré is $k_m = (k_{gr} - k_s)/(i - m) = (k_{gr} - k_s)/2$, and not $(k_{gr} - k_s)$ as is the case for the $i - m = 1$ moiré. The predominant intensity of the second harmonic $(k_{gr} - k_s)$ translates nothing else than the close (but not exact) lattice coincidence observed at half the moiré period (Fig. 1a bottom). The Fourier description of moirés naturally makes the distinction between both, the $i - m = 1$ moiré containing only one beating, and the $i - m = 2$ comprising two distinct ones.

The analysis of the moiré superlattices presented below will be performed by expressing the moiré superlattice unit vectors as function of those of the graphene and support unit cells. The analysis will also be expressed as function of elementary geometrical deformations, which we now introduce.

In the most general case, graphene is twisted, strained and sheared with respect to its substrate. The combination of all these contributions can be separated into four elementary geometrical transformations represented on Fig. 2a: an isotropic rescaling (1), a directional rescaling (2 and 3), and a rotation (4). These transformations translate in mechanical terms as biaxial strain ε_b (1), uniaxial strain in a given direction ε_u (2 and 3), and a rotation (4) of the graphene layer. It can be noted that the so far overlooked shearing contribution is taken into account by combining a rotation, biaxial and uniaxial strains. The impact of such a combination on a moiré has only been predicted[56].

On the other hand, one can equivalently describe the graphene-substrate relation by explicitly writing the commensurate relation defining the moiré superlattice. In order to account for its structural complexity in two dimensions, a set of eight integers (i, j, k, l, m, n, q, r), which are determined through atomically-resolved microscopy, is then necessary (only four are needed to describe graphene maintaining the D_{6h} symmetry, *i.e.* when it is only strained biaxially and rotated):

$$\begin{pmatrix}\mathbf{a}_{\mathbf{m}_1}\\ \mathbf{a}_{\mathbf{m}_2}\end{pmatrix} = M_{gr}\begin{pmatrix}\mathbf{a}_{\mathbf{gr}_1}\\ \mathbf{a}_{\mathbf{gr}_2}\end{pmatrix} = M_s\begin{pmatrix}\mathbf{a}_{\mathbf{s}_1}\\ \mathbf{a}_{\mathbf{s}_2}\end{pmatrix} \quad \text{with} \quad M_{gr} = \begin{pmatrix}i & j\\ k & l\end{pmatrix} \text{ and } M_s = \begin{pmatrix}m & n\\ q & r\end{pmatrix} \tag{1}$$

This translates into reciprocal space as (the "T" superscript denotes the transpose operation):

$$\begin{pmatrix}\mathbf{k}_{\mathbf{gr}_1}\\ \mathbf{k}_{\mathbf{gr}_2}\end{pmatrix} = M_{gr}^{T}\begin{pmatrix}\mathbf{k}_{\mathbf{m}_1}\\ \mathbf{k}_{\mathbf{m}_2}\end{pmatrix} \text{ and } \begin{pmatrix}\mathbf{k}_{\mathbf{s}_1}\\ \mathbf{k}_{\mathbf{s}_2}\end{pmatrix} = M_s^{T}\begin{pmatrix}\mathbf{k}_{\mathbf{m}_1}\\ \mathbf{k}_{\mathbf{m}_2}\end{pmatrix} \quad \text{with} \quad M_{gr}^{T} = \begin{pmatrix}i & k\\ j & l\end{pmatrix} \text{ and } M_s^{T} = \begin{pmatrix}m & q\\ n & r\end{pmatrix} \tag{2}$$

The (i, j, k, l, m, n, q, r) integers used here correspond to the decomposition of the superstructure lattice vectors $\mathbf{a}_{\mathbf{m}_1}$ and $\mathbf{a}_{\mathbf{m}_2}$ into the basis formed by the graphene lattice vectors (i, j, k, l), and the supporting material lattice vectors (m, n, q, r), as sketched on Fig. 2b. This decomposition is in practice performed more conveniently but equivalently in reciprocal space (Equation (2)).

By combining this description with that in terms of four geometrical transformations formally linking the graphene and support lattice vectors, one can relate the physical parameters describing how much graphene is strained and sheared to these eight integers. This relation is established in the Supplementary information (Equation (S21a,b)) and is later used to quantify uniaxial and biaxial strains in graphene.

At this point we can generalize to the two-dimensional limit the concept of number of beatings N in a moiré cell. One can then define number of beatings N_1 and N_2 along $\mathbf{a}_{\mathbf{m}_1}$ and $\mathbf{a}_{\mathbf{m}_2}$ (see Supplementary information):

$$N_1 = \sqrt{(i-m)^2 + (j-n)^2 - (i-m)(j-n)} \text{ and } N_2 = \sqrt{(k-q)^2 + (l-r)^2 - (k-q)(l-r)} \quad (3)$$

The number of beatings N within a moiré cell is then simply given by the product $N = N_1 N_2$.

Although using a set of eight integers is efficient to describe a moiré superlattice, it is a relatively cumbersome notation that does not give an immediate picture of the structure. A clearer formulation of such sheared structures is then desirable. In the simple case of graphene experiencing only deformations preserving its pristine D_{6h} symmetry, the Wood's notation circumvents this issue, describing the length and orientation of the superstructure lattice vectors compared to that of graphene or its supporting material. In the more general case addressed here, where the lattice vectors are allowed to vary in length and orientation independently as a result of shear and/or uniaxial strains, an extension of the Wood's notation is required, which we derive here. As depicted on Fig. 2c, $\mathbf{a}_{\mathbf{gr}_1}$ and $\mathbf{a}_{\mathbf{gr}_2}$ are rescaled (resp. rotated) with respect to $\mathbf{a}_{\mathbf{s}_1}$ and $\mathbf{a}_{\mathbf{s}_2}$ by factors p_1 and p_2 (resp. angles φ_1 and φ_2). The extended Wood's notation reads as $(p_1 \mathbf{R}\varphi_1 \times p_2 \mathbf{R}\varphi_2)$. This notation gives the reader the ability to easily capture the graphene-substrate relation, and imagine how sheared it is by comparing p_1 and p_2, and φ_1 and φ_2. Once again, these quantities relate to the (i, j, k, l, m, n, q, r) integers, as explained in the Supplementary information. The same can be done to relate the moiré unit vectors to those of the support, as $(P_1 \mathbf{R}\Phi_1 \times P_2 \mathbf{R}\Phi_2)$, with:

$$\begin{cases} p_1 = \sqrt{a^2 + b^2 - ab} & (4a) \\ \varphi_1 = \arctan\left(\dfrac{b\sqrt{3}}{2a - b}\right) & (4b) \\ p_2 = \sqrt{c^2 + d^2 - cd} & (4c) \\ \varphi_2 = \arctan\left(\dfrac{c\sqrt{3}}{c - 2d}\right) & (4d) \end{cases} \text{ and } \begin{cases} P_1 = \sqrt{m^2 + n^2 - mn} & (5a) \\ \Phi_1 = \arctan\left(\dfrac{n\sqrt{3}}{2m - n}\right) & (5b) \\ P_2 = \sqrt{q^2 + r^2 - qr} & (5c) \\ \Phi_2 = \arctan\left(\dfrac{q\sqrt{3}}{q - 2r}\right) & (5d) \end{cases}$$

with $a = \frac{lm - jq}{il - jk}, b = \frac{ln - jr}{il - jk}, c = \frac{iq - km}{il - jk}, d = \frac{ir - kn}{il - jk}$.

Precision on the structure determination. The geometrical formalism developed so far proves necessary to properly interpret the refined twist angles and shearings observed in atomically-resolved microscopy images. The experimental uncertainty on the identification of the (i, j, k, l, m, n, q, r) integers is here discussed to justify this necessity.

Quantitatively, the uncertainty on (i, j, k, l) can be lowered by precisely determining $(\mathbf{k}_{\mathbf{gr}_1}, \mathbf{k}_{\mathbf{gr}_2})$ and $(\mathbf{k}_{\mathbf{m}_1}, \mathbf{k}_{\mathbf{m}_2})$. In practice, we measure the distance between the moiré spots and the graphene spots in the Fourier transform image (each spot corresponding to a Fourier component), which are expected to be evenly separated. The sharpness of the spots is inversely proportional to the size of the atomically resolved image, and the number of spots increases with the contrast of the moiré with respect to the atomic lattice. The former effect sets a precision in the determination of the spacing between two spots of 6% in the case of gr/Ir, for which the image field of view is ~500 nm^2. The latter effect translates into an uncertainty as low as $1/\sqrt{50} \times 6\% \sim 1\%$ in the case of gr/Ir (see Results below). Indeed, around the center of the reciprocal space, there are ~60 Fourier components, which corresponds to ~50 Fourier component spacings along one direction. The same is true around the graphene harmonics, so overall, in our example, the precision over k_m and k_{gr} is ~1%. For (i, j, k, l), this precision translates through propagation of uncertainty into 2%.

The above described determination of (i, j, k, l, m, n, q, r) is liable to put shears in evidence. At first thought, atomic resolution imaging can artificially produce sheared images. Such shears may result from imaging artefacts, for instance, in the case of scanning probe microscopy, thermal drift of the piezoelectric scanners or inequivalent calibration of these scanners along the two scan directions. However, these artefacts have no influence on the decomposition of $\mathbf{k}_{\mathbf{gr}_1}$ and $\mathbf{k}_{\mathbf{gr}_2}$ onto $\mathbf{k}_{\mathbf{m}_1}$ and $\mathbf{k}_{\mathbf{m}_2}$.

Twisted graphene bilayer. First, the case of multilayer graphene on the C-rich $(000\bar{1})$ face (C-face) of a 4H-SiC sample is considered in Fig. 3, where a ~1.5 nm beating is observed. In the present case, the relationship between the lattice vectors of the upper graphene layer and of the moiré can be read on Fig. 3b to deduce matrix $M^{\mathrm{T}}_{\mathrm{gr_{up}}}$ (see Equation (2)). Here, this matrix indicates the coincidence of the graphene and moiré lattices in reciprocal space. In direct space, this means that the beatings match the moiré, so $N = 1$ (see General framework). For a $N = 1$ moiré, $\mathbf{k}_{\mathbf{m}_1} = \mathbf{k}^{\mathbf{up}}_{\mathbf{gr}_1} - \mathbf{k}^{\mathbf{low}}_{\mathbf{gr}_1}$, as the lower layer of graphene is the support material. From this, the matrix $M^{\mathrm{T}}_{\mathrm{gr_{low}}}$ between the lattice vectors of the lower graphene layer and of the moiré is obtained. Transposing matrices $M^{\mathrm{T}}_{\mathrm{gr_{up}}}$ and $M^{\mathrm{T}}_{\mathrm{gr_{low}}}$ gives $M_{\mathrm{gr_{up}}}$ and $M_{\mathrm{gr_{low}}}$, which hold the decomposition of the moiré unit vectors on the upper and lower graphene lattices in direct space:

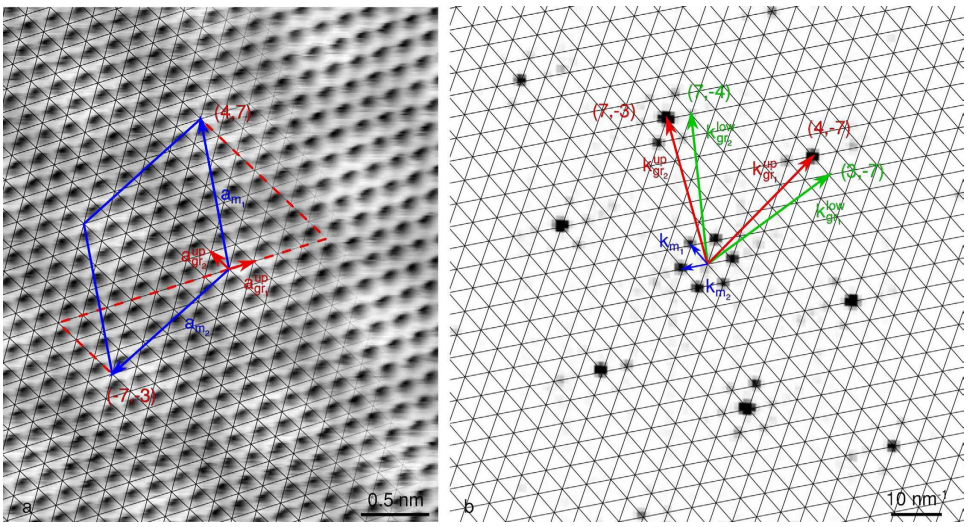

Figure 3. STM analysis of multilayer graphene on C-face SiC: (**a**) ($3.2 \times 3.8\,\mathrm{nm}^2$) STM topograph ($I_{\mathrm{tunnel}} = 10\,\mathrm{nA}$, $V_{\mathrm{bias}} = 100\,\mathrm{mV}$) with emphasized upper graphene lattice (black), moiré superlattice cell (blue rhombus) and lattice vectors of upper graphene and moiré (red and blue respectively). (**b**) Corresponding FFT-image with emphasized moiré reciprocal lattice (black) and lattice vectors of moiré and upper and lower layers of graphene (blue, red and green respectively).

$$M^{\mathrm{T}}_{\mathrm{gr_{up}}} = \begin{pmatrix} 4 & -7 \\ 7 & -3 \end{pmatrix} \text{ and } M^{\mathrm{T}}_{\mathrm{gr_{low}}} = \begin{pmatrix} 3 & -7 \\ 7 & -4 \end{pmatrix} \text{ so } M_{\mathrm{gr_{up}}} = \begin{pmatrix} 4 & 7 \\ -7 & -3 \end{pmatrix} \text{ and } M_{\mathrm{gr_{low}}} = \begin{pmatrix} 3 & 7 \\ -7 & -4 \end{pmatrix}$$

This commensurability relation gives a complete structural description, by decomposing the moiré lattice vectors in the basis of each graphene layer, using the set of integers $(i, j, k, l, m, n, q, r) = (4, 7, -7, -3, 3, 7, -7, -4)$. Using Equation (4a–d), such a structure can be analysed as two graphene layers sharing the same lattice parameter $a^{\mathrm{up}}_{\mathrm{gr}} = a^{\mathrm{low}}_{\mathrm{gr}}$ ($p_1 = p_2 = 1$), and rotated by $\varphi = \varphi_1 = \varphi_2 = \arctan(7\sqrt{3}/73) \sim 9.43°$ with respect to each other. This falls in the regime where the two graphene layers interact weakly, leading to Fermi velocity renormalization around the Dirac cones[23,28,29].

Graphene on Re(0001). The case of multilayer graphene on C-face SiC has shown a situation where a moiré superlattice is related to a single structural parameter: the twisting angle φ. On the contrary, graphene supported by a metallic surface can not only be twisted with respect to its substrate, but also strained, due to the lattice mismatch between the two. A full monolayer of graphene forms on Re(0001) through a self-limiting process[58], and a ~2.2 nm period beating is found. These beatings were described as a $N = 1$ moiré superlattice with 10 graphene cells on 9 Re cells[59], or 8 graphene cells on 7 Re cells[32].

A direct analysis of the STM topograph along the same lines as for Fig. 3 is here challenging. Figure 4a highlights two additional phenomena, which have been little discussed to our knowledge in the context of graphene on metals[60].

First, depending on the position within the beatings, the apparent height accessed by STM shows a varying number of visible C: in a valley, only 3 atoms out of a 6-C ring are seen, whereas on a hill, all 6 are observed. This is due to the sites occupied by the C atoms on the terminal metallic layer, which fall into three typical configurations: a C on top of a metal atom (atop), or on top of a hollow site. Two kinds of hollow site can be distinguished, depending on the presence (hcp) or absence (fcc) of another metal atom of the second terminal metallic layer below the hollow site. In a valley, the sites occupied by the C atoms are either atop and hcp, or atop and fcc. The overlap of the p_z-like orbital of a C atom in atop position with the d-like orbitals of the underlying metal atom is then maximal. Consequently, the local electronic density of states is modified, making it appear low in STM[10]. This explains why, for strongly-interacting substrates, only half the C atoms appear as protrusions in a moiré valley, while all of them can be identified on top of a moiré hill (see refs 38,51,60,61 for gr/Ru, ref. 62 for gr/Rh, and ref. 32 for gr/Re).

Second, the apparent atomic rows of C oscillate with the same periodicity as the beatings. This phenomenon has been reported and discussed in the case of gr/Ru (see ref. 60), and observed as well in many instances before and since then, it is known since the 1990s as the "odd-even transition" in the case of graphite[63–65]. Its origin is well illustrated in the case of the two distinctive moiré valleys. Indeed, they differ only in the site of the remaining visible C atom: hcp or fcc. Depending on whether the site is hcp or fcc, the corresponding C atom belongs to sub-lattice A or B of graphene. As a consequence, when moving from one beating to the other, the C atoms that are observed switch continuously from one sub-lattice to the other. Along a row of C atoms, this induces an apparent oscillation of the row. Therefore, these two effects are related to a modulation of the electronic density of states on the two sub-lattices of graphene, which is correlated with the moiré periodicity.

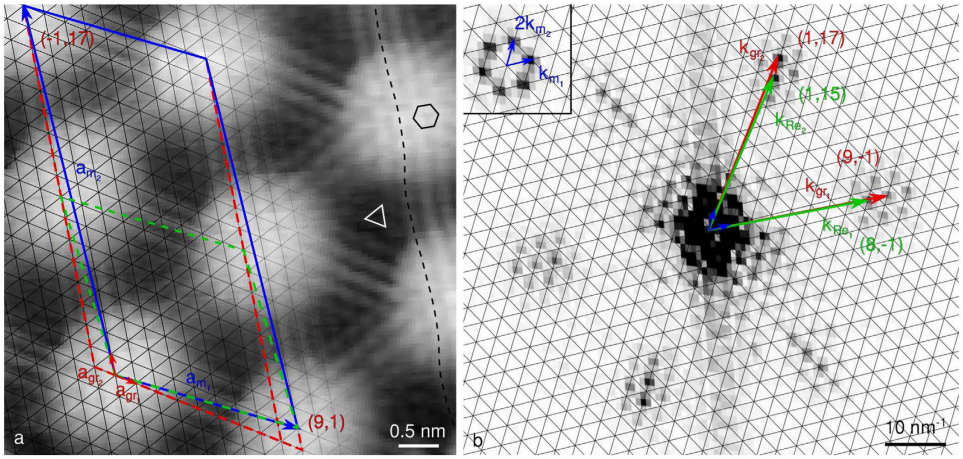

Figure 4. STM analysis of gr/Re: (**a**) ($5.6 \times 5.2\,nm^2$) STM topograph ($I_{tunnel} = 6\,nA$, $V_{bias} = 30\,mV$) with overlaid graphene lattice (black), and lattice vectors of graphene and $N = 2$ superlattice (red and blue arrows respectively). Moiré cell (blue full line) and its closest unsheared approximation with $N = 1$ beating (green dashed line), with the coordinates of its corners in the graphene basis. The "odd-even" transition along lines of carbon atoms is also emphasized, as well as the either 6 or 3 C atoms observed in a moiré hill or valley. (**b**) Corresponding FFT-image with emphasized moiré reciprocal lattice (black) and lattice vectors of moiré, graphene and Re (blue, red and green respectively). Inset shows the $\mathbf{k_{gr}} - \mathbf{k_{Re}}$ harmonics surrounding the center of the FFT-image with improved contrast.

Using DFT calculations, these two effects have been reproduced in the case of a sheared and twisted $N = 1$ moiré superlattice of gr/Re, comprising a sufficiently small number of atoms to be treated numerically. This moiré is characterized by the set $(i, j, k, l, m, n, q, r) = (9, 3, -2, 7, 8, 3, -2, 6)$. On Fig. S2b, one can see that the moiré reproduces the two anomalies described above. Only one C sub-lattice is observed in each moiré valley. Within the unit cell, this causes an effective oscillation of the atomic C row, which is actually related to the varying contribution of each sub-lattice to the electronic density, as can be checked on Fig. S2a.

On Fig. S2b, it can be noted that the hills of the beating are not circular, but appear rather elliptical. This is attributed to the small shearing that graphene undergoes in this superstructure, whose effect is enhanced on the moiré. Similar non-circular hills can be observed on Fig. 4a, which is another clue that indicates graphene structure is sheared on this STM topograph.

Figure 4a,b display an analysis taking the two STM electronic effects into account. The FFT image is analysed similarly to Fig. 3b, although the situation is different. Indeed, in two directions, the graphene spots do not superimpose with the extrapolated reciprocal space lattice paved with the $\mathbf{k_{gr_1}} - \mathbf{k_{Re_1}}$ and $\mathbf{k_{gr_2}} - \mathbf{k_{Re_2}}$ vectors. This means that the moiré is not a $N = 1$ superlattice (cf. Fig. 1a bottom,b). Moreover, the positions of the graphene spots with respect to the moiré reciprocal network vary for the three main directions. Consequently, based on the reciprocal space analysis, the moiré structure considered here is sheared. The commensurability relation of this structure reads as:

$$M_{gr}^{T} = \begin{pmatrix} 9 & -1 \\ 1 & 17 \end{pmatrix} \text{ and } M_{Re}^{T} = \begin{pmatrix} 8 & -1 \\ 1 & 15 \end{pmatrix} \text{ so } M_{gr} = \begin{pmatrix} 9 & 1 \\ -1 & 17 \end{pmatrix} \text{ and } M_{Re} = \begin{pmatrix} 8 & 1 \\ -1 & 15 \end{pmatrix}$$

The corresponding set of integers therefore is $(i, j, k, l, m, n, q, r) = (9, 1, -1, 17, 8, 1, -1, 15)$. As a signature of the anisotropy, the moiré cell contains a different number of beatings $N_1 = 1$ and $N_2 = 2$ in each of its main directions, as can be deduced from Equation (3). This analysis is displayed in direct space on top of the original STM topograph on Fig. 4a, where the superstructure lattice vectors are explicitly decomposed on the graphene lattice.

To get a more simple grasp of this structure, the moiré can be described using the $(P_1\,\mathbf{R}\Phi_1 \times P_2\,\mathbf{R}\Phi_2)$ extended Wood's notation, with $P_1 = \sqrt{8^2 + 1^2 - 1 \times 8} \sim 7.55$, $P_2 = \sqrt{(-1)^2 + 15^2 - (-1) \times 15} \sim 15.52$, $\Phi_1 = \arctan(\sqrt{3}/15) \sim 6.59°$, and $\Phi_2 = \arctan(\sqrt{3}/31) \sim 3.20°$, as deduced from Equation (5a–d). This notation makes clear the twice larger size of the moiré compared to a $N = 1$ superlattice, comprising 308 carbon atoms, as well as a sizeable shear. The corresponding shear of the graphene lattice is obvious in the corresponding extended Wood's notation $(p_1\,\mathbf{R}\varphi_1 \times p_2\,\mathbf{R}\varphi_2)$. Using Equation (4a–d), one gets $p_1 = \sqrt{137^2 + 2^2 - 2 \times 137}/154 \sim 0.883$, $p_2 = \sqrt{(-1)^2 + 136^2 + 1 \times 136}/154 \sim 0.886$, $\varphi_1 = \arctan(\sqrt{3}/136) \sim 0.73°$ and $\varphi_2 = \arctan(\sqrt{3}/271) \sim 0.36°$. This is summarized as $(0.883\,\mathbf{R}0.73 \times 0.886\,\mathbf{R}0.36)$. This structure is close but different from the previously reported assignment of a $(7 \times 7)\mathbf{R}0$, $N = 1$ moiré (ref. 32).

Overall, the structure is a superlattice both sheared and twisted with $N_1 = 1$ beating in one direction and $N_2 = 2$ in the other, giving rise to $N = 2$ beatings in the moiré cell. This is significantly more complex than the $N = 1$ twisted superlattices discussed in many reports, and even than the $N = 4$ untwisted superlattices reported in gr/Ir (see ref. 66) and gr/Ru (see ref. 51), or than a solely sheared superlattice[56].

A more physical description of such a structure is given by comparing the graphene overlayer with its HOPG counterpart, and decomposing the strain in terms of a uniaxial and a biaxial contributions. Using Equation

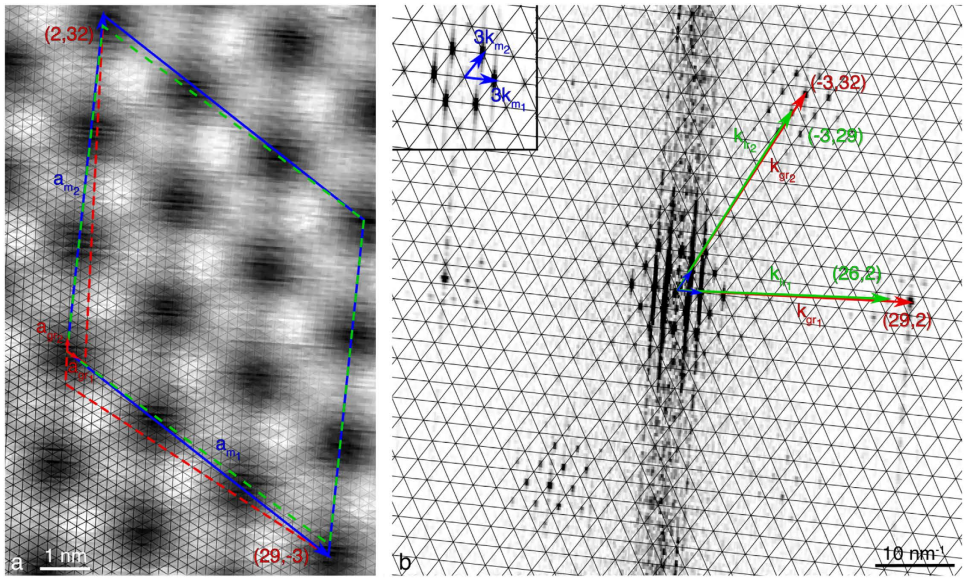

Figure 5. STM analysis of gr/Ir: (**a**) ($13.5 \times 7.4\,nm^2$) STM topograph ($I_{tunnel} = 20\,nA$, $V_{bias} = 60\,mV$) with highlighted graphene lattice (black), and lattice vectors of graphene and $N = 9$ moiré (red and blue arrows respectively). Moiré cell (blue line) with the coordinates of its corners in the graphene basis, and its closest unsheared approximation (green dashed line). It should be noted the contrast is inverted compared to Fig. 4, so hills appear as dark. (**b**) FFT-image obtained from a $15.6 \times 30\,nm^2$ STM topograph, and overlaid with the lattice paved with $\mathbf{k_{gr}} - \mathbf{k_{Ir}}$ vectors, and lattice vectors of moiré, graphene and Ir (blue, red and green respectively). Inset shows moiré spots surrounding the center of the FFT-image with improved contrast.

(S21a,b) in the case of gr/Re, graphene is biaxally compressed by $\varepsilon_b \sim -0.14\%$ and uniaxially compressed by $\varepsilon_u \sim -0.84\%$. This shows a moiré is actually related to a non-trivial distortion of the graphene lattice.

Graphene on Ir(111). The anisotropy of the graphene and moiré lattices is also encountered when the graphene-substrate interaction is much weaker, *e.g.* in the case of gr/Ir. Similarly to gr/Re, the FFT-image of Fig. 5b shows the graphene spots do not superimpose with the extrapolated reciprocal lattice paved with $\mathbf{k_{gr_1}} - \mathbf{k_{Ir_1}}$ and $\mathbf{k_{gr_2}} - \mathbf{k_{Ir_2}}$, which means the moiré comprises more than a single beating ($N > 1$). In addition, the position of the graphene spots with respect to the moiré reciprocal lattice is not the same in each main direction, which means the structure is sheared. Actually, along the close-to-horizontal direction in reciprocal space (center-right in Fig. 5b), the set of harmonics around $\mathbf{k_{gr_1}}$ are for instance found right at the center of mass of the triangles defined by the extrapolated lattice. On the contrary, for the second direction (top-right in Fig. 5b), the set of harmonics around $\mathbf{k_{gr_2}}$ lies in between two nodes of the extrapolated reciprocal lattice. This translates into the commensurability relation as:

$$M_{gr}^{T} = \begin{pmatrix} 29 & 2 \\ -3 & 32 \end{pmatrix} \text{ and } M_{Ir}^{T} = \begin{pmatrix} 26 & 2 \\ -3 & 29 \end{pmatrix} \text{ so } M_{gr} = \begin{pmatrix} 29 & -3 \\ 2 & 32 \end{pmatrix} \text{ and } M_{Ir} = \begin{pmatrix} 26 & -3 \\ 2 & 29 \end{pmatrix}$$

This description of the superlattice can be summarized with $(i, j, k, l, m, n, q, r) = (29, -3, 2, 32, 26, -3, 2, 29)$, as interpreted in Fig. 5a. Such a moiré comprises three beatings in each direction (Equation (3)), in total 1,868 carbon atoms. In the extended Wood's notation, this superlattice is described with $(P_1\,\mathbf{R}\Phi_1 \times P_2\,\mathbf{R}\Phi_2)$, with $P_1 = \sqrt{26^2 + (-3)^2 + 26 \times 3} \sim 27.62$, $P_2 = \sqrt{2^2 + 29^2 - 2 \times 29} \sim 28.05$, $\Phi_1 = \arctan(-3\sqrt{3}/55) \sim -5.40°$, and $\Phi_2 = \arctan(-\sqrt{3}/28) \sim -3.54°$, as deduced from Equations (5a–d). This is very close but still different from the so-called incommensurate (9.32×9.32) **R**0° structure[36]. The graphene structure is similarly described with $(p_1\,\mathbf{R}\varphi_1 \times p_2\,\mathbf{R}\varphi_2)$, with $p_1 = \sqrt{838^2 + (-9)^2 - 838 \times (-9)}/934 \sim 0.902$, $p_2 = \sqrt{6^2 + 847^2 - 6 \times 847}/934 \sim 0.904$, $\varphi_1 = \arctan(-9\sqrt{3}/1685) \sim -0.53°$, and $\varphi_2 = \arctan(-3\sqrt{3}/844) \sim -0.35°$, as deduced from Equation (4a–d). These values are in excellent agreement with the 0.903 ratio recently measured by means of surface X-ray scattering[67].

Using Equation (S21a,b), this shearing translates into a combination of biaxial compression $\varepsilon_b \sim -0.29\%$ and uniaxial compression $\varepsilon_u \sim -0.41\%$ (expressed using HOPG as a reference for unstrained graphene). Shear and strain of such extents have already been reported before[49], but no quantitative analysis was provided.

Discussion

Three support lattices have been considered so far, revealing that a moiré structure can be rotated, strained and sheared. It also demonstrates that moiré superlattices comprising more than one beating are commonly encountered. Three equivalent ways have been presented to describe moiré superlattices with ease:

- Using an extended Wood's notation for a pictorial description using two scaling factors and two angles,
- In more physical terms with rotation angles, and uniaxial and biaxial strains,
- With eight integers that decompose independently the two moiré lattice vectors onto those of graphene and of its support.

The use of such eight integers proves necessary for a universal description of all moiré superlattices, in particular of $N>1$ beatings superlattices, and of sheared superlattices, which both display specific properties. $N>1$ beatings superlattices indeed exhibit inequivalent moiré hills[52], whose different geometrical configurations result in differences in the local doping level of ~100 meV, which corresponds to ~10^{12} cm^{-2} (see ref. 32). Additionally, the geometrical description of a moiré superlattice has a direct link with the position of its replica bands and mini-gaps in reciprocal space. Angle-resolved photoemission spectroscopy[20,23] and Raman spectroscopy[68,69] probe the former, while conductance measurements[25–27] are a precise mean to measure the latter. If sufficiently sensitive and resolved, these techniques will detect the fundamental component of $N>1$ beatings superlattices.

As for sheared superlattices, their broken three-fold symmetry imposes a Brillouin zone with shifted K and K' points (with respect to pristine graphene), hence with shifted Dirac cones[70]. Upon large shear strains, they are predicted to merge, so a band gap opens. Additionally, even marginal shear strain should shift the wave-vector position of the superlattice mini-gaps. As a consequence, for twisted bilayer graphene, this broken-symmetry is predicted to give rise to multiple Van Hove singularities in the electronic density of states[71]. The geometrical analysis presented here is thus a tool towards the quantitative prediction of such effects.

The notation relying on eight integers enables to enumerate all the possible structures by combining every possible value for each integer. The system can also be treated by addressing two independent directions separately, *i.e.* by considering two sets of four integers, (i, j, m, n) and (k, l, q, r), which obey the same equations. Below, we introduce these equations in the case of (i, j, m, n) from Equations (1) and (2):

$$M_{gr} = \begin{pmatrix} i & j \\ -j & i-j \end{pmatrix},\ M_s = \begin{pmatrix} m & n \\ -n & m-n \end{pmatrix} \text{ and } M_{gr}^T = \begin{pmatrix} i & -j \\ j & i-j \end{pmatrix},\ M_s^T = \begin{pmatrix} m & -n \\ n & m-n \end{pmatrix} \tag{6}$$

Out of these two equivalent equations, and using only the support lattice constant a_s, one can express the moiré lattice constant a_m, the biaxial strain ε (assuming the lattice parameter of HOPG as a zero-strain situation), and the twist angle φ between graphene and its support (see Supplementary information):

$$\begin{cases} a_m = a_s\sqrt{m^2+n^2-mn} \\ \varepsilon = \dfrac{a_{gr}-a_{HOPG}}{a_{HOPG}} = \dfrac{a_s}{a_{HOPG}}\sqrt{\dfrac{m^2+n^2-mn}{i^2+j^2-ij}} - 1 \\ \varphi = \arctan\left(\dfrac{(in-jm)\sqrt{3}}{2(im+jn)-(in+jm)}\right) \end{cases} \tag{7}$$

The link with their Wood's notation $(p\times p)\ \mathbf{R}\varphi$ can be established straightforwardly (see Supplementary information) as:

$$p = \frac{a_{gr}}{a_s} = \sqrt{\frac{m^2+n^2-mn}{i^2+j^2-ij}} \text{ and } \varphi = (\mathbf{a_s}, \mathbf{a_{gr}}) = \arctan\left(\frac{(in-jm)\sqrt{3}}{2(im+jn)-(in+jm)}\right) \tag{8}$$

With increasing values of (i, j, m, n), it is then possible to enumerate every possible structure. Using a limited set of parameters such as those defined by Equation (8) allows for a graphical representation of the strain of every possible moiré superlattice in a given direction. Figure 6 gives this representation in the case of graphene on dense-packed surfaces of Ir and Pt (see Supplementary information for Re). Figure 6 also displays parametrized curves accounting for a definition of a moiré superlattice with no assumption on commensurability, corresponding to the one-dimensional formula $Nk_m = k_{gr} - k_s$. The representation of these curves is given by:

$$a_m = a_s\sqrt{\frac{N}{1-2p\ \cos\ \varphi+p^2}} \tag{9}$$

where $p = \frac{a_{gr}}{a_s} = \frac{a_{HOPG}}{a_s}(\varepsilon+1)$ and N the number of beatings given by Equation (3) with $N_1 = N_2$.

This series of parametrized curves highlights moiré superlattices with increasing numbers of beatings N (see Supplementary information). The above-described results, as well as data extracted from the literature in the case of gr/Pt and gr/Ir, are displayed on Fig. 6.

In the case of gr/Pt (Fig. 6b), the interpretation in terms of sub-3 nm period superlattices corresponds to suspiciously high strains for a system with such a weak interaction between graphene and the metal. For instance, the phases of gr/Pt indexed as 11, 19, 20 and 21 on Fig. 6b have been interpreted as moiré superlattices with respectively $\varepsilon = 2.51\%$ (11), $\varepsilon = -1.73\%$ (19) and $\varepsilon = 3.45\%$ (20), and $\varepsilon = -2.38\%$ (21). Higher number of beatings are in fact probable for such structures. Such a high number of beatings was determined in the case of the so-called R30 phase of gr/Ir (see ref. 43). A combined micro-spot low energy electron diffraction (μ-LEED) and STM study showed that within a moiré unit cell of ~3.02 nm lattice parameter, $N = 37$ beatings separated by ~0.47 nm occur ($N_1 = N_2 = \sqrt{37}$). This $N = 37$ moiré is described with $(i, j, m, n) = (14, 9, 12, 2)$ (indexed as 9 on Fig. 6a), which corresponds to $\varepsilon = -0.04\%$. This moiré was also described as a $N = 1$ moiré[46] with $(i, j, m, n) = (2, 0, 2, 1)$ (indexed

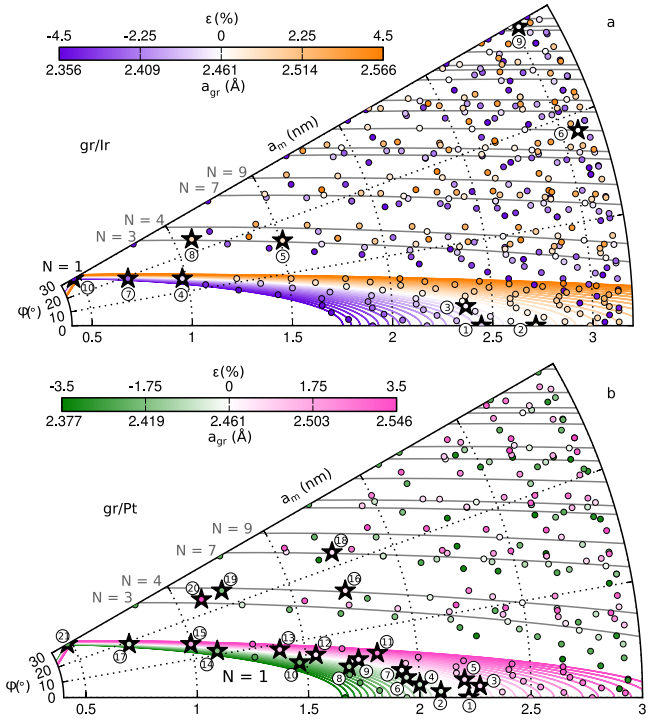

Figure 6. Moiré lattice constant a_m versus angle φ between graphene and its support. Each point corresponds to a commensurate superlattice of given a_m and φ, with its colour indicating the strain level of graphene. The full lines indicate the superlattices containing N beatings within the moiré cell. The coloured ones add a strain information, and for clarity are only shown for the $N=1$ case. (**a**) gr/Ir, (**b**) gr/Pt (with lattice parameters $a_{Ir}=2.7147$ Å and $a_{Pt}=2.7744$ Å, see ref. 18). Black stars index reported unsheared structures (see Supplementary information for detailed references).

as 10 on Fig. 6a), for which $\varepsilon=-4.48\%$, which is questionable. Similarly, the so-called R18.5 of gr/Ir was interpreted as either $(i, j, m, n)=(13, 1, 13, 5)$, $\varepsilon=-0.02\%$ (ref. 43), or $(i, j, m, n)=(3, 0, 3, 1)$, $\varepsilon=-2.73\%$ (ref. 72), respectively labelled as 6 and 7 on Fig. 6a.

The analysis performed here demonstrates the rich variety of moiré superlattices to be expected for graphene on a substrate, well beyond the simple case of $N=1$ unsheared cases. Although many structures are possible from the geometrical point of view, few of them have actually been reported in the literature. This state of fact can be interpreted in two different ways: either differentiating some very similar structures has not been considered or is not possible due to too limited space resolution, or only a few of them are stable enough to actually exist.

Gr/Ir and gr/Pt are typical of the first situation. Numerous moiré phases have been reported for them, as shown on Fig. 6a,b. The majority of them is identified as $N=1$ moiré superlattices, nevertheless, this description appears sometimes unrealistic. For gr/Re, like gr/Ru and gr/Ni, graphene tends to align its zigzag rows to the close-packed rows of the metal ($\varphi\sim0°$), even in growth conditions quite far from thermodynamic equilibrium. Presumably, the strong bonds of covalent character between carbon and metal atoms inside the growing flake are not readily broken, as would be required for twisting.

Although large-angle graphene twists are almost prohibited for gr/Re, slightly twisted graphene phases of gr/Re coexist. These numerous very similar structures can be assumed to be local minima in the energy landscape of gr/Re. Their coexistence then implies a high activation energy between each of them, so the formation of a large-scale uniform graphene phase is kinetically limited. In other words, graphene needs to be heated to high enough temperature to rearrange into the most stable phase of gr/Re. However, at high temperature, graphene growth competes with bulk dissolution and carbide formation, so the growth is performed by annealing cycles[58]. Over each cycle, graphene's crystallinity progressively improves, which supports this simple kinetic scenario. To go further, one can compare this situation with that of gr/Ru, where domains slightly rotated around $\varphi\sim0°$ can be grown, as observed in STM[73] and μ-LEED[74]. By tuning the growth to higher temperature, large domains of one specific structure tend to form[61,73], which has been analysed as a $N=4$ ($N_1=N_2=2$) superlattice ($(i, j, m, n)=(25, 0, 23, 0)$) using surface x-ray diffraction[51]. Such similar behaviours may lead to the conclusion that the mechanism presented here is common to every system where graphene is in strong interaction with its substrate.

Graphene on C-face SiC grows with rotational disorder between the adjacent graphene layers[75], so the terminal layers exhibit many possible twisted phases[76]. Even though all kinds of twists are encountered in experiments, it seems that certain twist angles are preferential. We surmise that these twist angles correspond to commensurate moiré superlattices such as the one that we report. Since both graphene layers share the same lattice parameter, the situation can be depicted with two integers (i, j), such that $(i, j, m, n)=(i, j, -j, i-j)$. For instance, $(i, j)=(4, 7)$ in the present work, and $(i, j)=(4, 1)$ in ref. 75. We note that the observation, with diffraction techniques, of a

continuum of twist angles (e.g. see ref. 75) does not necessarily imply that the twist angle can take random values. Indeed, the existence of a multitude of commensurate superlattices discretely spanning the $0-60°$ twist range could as well account for the observation due to the finite size of the diffraction spot (set by the domain size or the instrumental resolution) that they yield.

In conclusion, different supported graphene systems have been studied with STM. A consistent analysis of moiré superlattices involving both direct and FFT STM images has been presented. The geometry of the superlattices, as apparent in STM images, has been rationalized by calculating electronic density maps derived from DFT calculations. A spatial precision of a tenth of 1 pm is achieved, revealing that graphene lying on a substrate is actually twisted, strained and sheared, which breaks its rotational symmetry. A geometrical model enables to classify all moiré superlattices. This model gives a global picture assuming commensurability between graphene and its substrate (and consequently between graphene or the substrate, and the moiré), yielding various numbers of beatings. While a very large number of structures is possible, only a few have actually been reported. In the case of strong graphene-substrate interaction, it is unlikely that all predicted superlattices are discovered, since for instance phases corresponding to a substantial rotation of graphene with respect to the substrate do not tend to form. For low interaction graphene-substrate systems, the complexity of the moiré superlattices has been undetected or overlooked, leading to possibly simplified interpretations. We anticipate that moiré superlattices with $N > 1$ number of beatings will produce rich electronic modulations in graphene.

Methods

Preparation of multilayer gr/SiC. Graphene has been grown on undoped double-polished 4H-SiC(000$\bar{1}$), purchased from Novasic and cut into $5 \times 5\,mm^2$ pieces. The growth has been performed in a RF-furnace following the recipe in ref. 77. SiC surface was first cleaned in H_2 and Ar atmosphere at 1,560 °C, and subsequently annealed in Ar atmosphere at the same temperature.

Preparation of gr/Re. Re single crystal cut in the (0001) surface purchased from Surface Preparation Laboratory was cleaned in a ultrahigh vacuum (UHV) chamber (base pressure $\sim 10^{-10}$ mbar) by cycles of Ar^+ ion bombardment at 2 keV at 750 °C and subsequent annealing at ~1,300 °C. The gr/Re was prepared following the recipe presented in ref. 58, by saturating the Re(0001) surface with C_2H_4 at room temperature (introduced with a $3 \cdot 10^{-8}$ mbar pressure), and two subsequent cycles of flash-annealing/cooling at 750 °C with a $5 \cdot 10^{-7}$ mbar C_2H_4 pressure.

Preparation of gr/Ir. An Ir single crystal cut in the (111) surface purchased from Surface Preparation Laboratory was cleaned in the same UHV chamber as for gr/Re, by cycles of Ar^+ ion bombardment at 1 keV and subsequent annealing at 1,200 °C. The gr/Ir was prepared by exposing to 10^{-8} mbar of C_2H_4 at 1,000 °C for 15 minutes.

STM measurements. For multilayer gr/SiC, STM measurements were performed at 4 K in a home-made He-cooled STM, using a commercial Pt/Ir tip bought from Bruker. For gr/Re and gr/Ir, STM measurements were performed at room temperature under UHV, using a commercial Omicron UHV-STM 1, with a W chemically etched tip. Before analysing STM images, thermal drift and miscalibrations have been corrected.

DFT calculations. DFT calculations were performed using the VASP code, with the projector augmented wave (PAW) approach[78,79]. The exchange correlation interaction is treated within the general gradient approximation parameterized by Perdew, Burke and Ernzerhof (PBE)[80]. The Methfessel Paxton method is used to calculate the total energy with a smearing of 0.2. The cut-off energy is of 400 eV. The supercell consists in four Re layers and one C layer with an empty space of 9 Å to avoid spurious interactions. Re atoms are kept fixed in the bottom second Re layer, all other atoms are allowed to relax. Due to the size of the supercell, calculations are performed using the K point only. After convergence, residual forces are lower than 0.03 eV/Å.

References

1. Wallace, P. The band theory of graphite. *Phys. Rev.* **71,** 622–634 (1947).
2. Semenoff, G. W. Condensed-matter simulation of a three-dimensional anomaly. *Phys. Rev. Lett.* **53,** 2449 (1984).
3. Novoselov, K. S. *et al.* Two-dimensional gas of massless Dirac fermions in graphene. *Nature* **438,** 197–200 (2005).
4. Wintterlin, J. & Bocquet, M.-L. Graphene on metal surfaces. *Surf. Sci.* **603,** 1841–1852 (2009).
5. First, P. N. *et al.* Epitaxial graphenes on SiC. *MRS Bulletin* **35,** 296–305 (2010).
6. Riedl, C., Coletti, C. & Starke, U. Structural and electronic properties of epitaxial graphene on SiC(0001): a review of growth, characterization, transfer doping and hydrogen intercalation. *J. Phys. D: Appl. Phys.* **43,** 374009 (2010).
7. Batzill, M. The surface science of graphene: Metal interfaces, CVD synthesis, nanoribbons, chemical modifications, and defects. *Surf. Sci. Rep.* **67,** 83–115 (2012).
8. Tetlow, H. *et al.* Growth of epitaxial graphene: theory and experiment. *Phys. Rep.* **542,** 195–295 (2014).
9. Dedkov, Y. & Voloshina, E. Graphene growth and properties on metal substrates. *J. Phys. Condens. Matter* **27,** 303002 (2015).
10. Wang, B., Bocquet, M.-L., Marchini, S., Günther, S. & Wintterlin, J. Chemical origin of a graphene moiré overlayer on Ru(0001). *Phys. Chem. Chems. Phys.* **10,** 3530 (2008).
11. Brako, R., Šokčević, D., Lazić, P. & Atodiresei, N. Graphene on the Ir(111) surface: from van der Waals to strong bonding. *New J. Phys.* **12,** 113016 (2010).
12. Busse, C. *et al.* Graphene on Ir(111): physisorption with chemical modulation. *Phys. Rev. Lett.* **107,** 036101 (2011).
13. Vita, H. *et al.* Understanding the origin of band gap formation in graphene on metals: graphene on Cu/Ir(111). *Sci. Rep.* **4,** 5704 (2014).
14. Voloshina, E. N. & Dedkov, Y. S. General approach to understanding the electronic structure of graphene on metals. *Mater. Res. Express* **1,** 035603 (2014).
15. Dean, C. R. *et al.* Boron nitride substrates for high-quality graphene electronics. *Nature Nanotech.* **5,** 722–726 (2010).
16. Hass, J. *et al.* Structural properties of the multilayer graphene/4H-SiC(000$\bar{1}$) system as determined by surface x-ray diffraction. *Phys. Rev. B* **75,** 214109 (2007).

17. Haigh, S. J. *et al.* Cross-sectional imaging of individual layers and buried interfaces of graphene-based heterostructures and superlattices. *Nature Mater.* **11,** 764–767 (2012).
18. King, H. W. *CRC Handbook Of Chemistry And Physics* (eds Lide, D. R.) Ch. 12, 10–12 (CRC press, 74th edition, 1993–1994).
19. Orlita, M. *et al.* Approaching the Dirac point in high-mobility multilayer epitaxial graphene. *Phys. Rev. Lett.* **101,** 267601 (2008).
20. Pletikosić, I. *et al.* Dirac cones and minigaps for graphene on Ir(111). *Phys. Rev. Lett.* **102,** 056808 (2009).
21. Ortix, C., Yang, L. & van den Brink, J. Graphene on incommensurate substrates: trigonal warping and emerging Dirac cone replicas with halved group velocity. *Phys. Rev. B* **86,** 081405(R) (2012).
22. Yankowitz, M. *et al.* Emergence of superlattice Dirac points in graphene on hexagonal boron nitride. *Nature Phys.* **8,** 382–386 (2012).
23. Ohta, T. *et al.* Evidence for interlayer coupling and moiré periodic potentials in twisted bilayer graphene. *Phys. Rev. Lett.* **109,** 186807 (2012).
24. Park, C.-H., Yang, L., Son, Y.-W., Cohen, M. L. & Louie, S. G. New generation of massless Dirac fermions in graphene under external periodic potentials. *Phys. Rev. Lett.* **101,** 126804 (2008).
25. Ponomarenko, L. A. *et al.* Cloning of Dirac fermions in graphene superlattices. *Nature* **497,** 594–597 (2013).
26. Hunt, B. *et al.* Massive Dirac fermions and Hofstadter butterfly in a van der Waals heterostructure. *Science* **340,** 1427–1430 (2013).
27. Dean, C. R. *et al.* Hofstadter's butterfly and the fractal quantum Hall effect in moiré superlattices. *Nature* **497,** 598–602 (2013).
28. Luican, A. *et al.* Single-layer behavior and its breakdown in twisted graphene layers. *Phys. Rev. Lett.* **106,** 126802 (2011).
29. Trambly de Laissardière, G., Mayou, D. & Magaud, L. Numerical studies of confined states in rotated bilayers of graphene. *Phys. Rev. B* **86,** 125413 (2012).
30. Stradi, D. *et al.* Role of dispersion forces in the structure of graphene monolayers on Ru surfaces. *Phys. Rev. Lett.* **106,** 186101 (2011).
31. Gao, M. *et al.* Epitaxial growth and structural property of graphene on Pt(111). *Appl. Phys. Lett.* **98,** 033101 (2011).
32. Tonnoir, C. *et al.* Induced superconductivity in graphene grown on rhenium. *Phys. Rev. Lett.* **111,** 246805 (2013).
33. Ugeda, M. M. *et al.* Point defects on graphene on metals. *Phys. Rev. Lett.* **107,** 116803 (2011).
34. Sutter, P., Hybertsen, M. S., Sadowski, J. T. & Sutter, E. Electronic structure of few-layer epitaxial graphene on Ru(0001). *Nano Lett.* **9,** 2654–2660 (2009).
35. Papagno, M. *et al.* Large band gap opening between graphene Dirac cones induced by Na adsorption onto an Ir superlattice. *ACS Nano* **6,** 199–204 (2012).
36. N'Diaye, A. T., Coraux, J., Plasa, T. N., Busse, C. & Michely, T. Structure of epitaxial graphene on Ir(111). *New J. Phys.* **10,** 043033 (2008).
37. Donner, K. & Jakob, P. Structural properties and site specific interactions of Pt with the graphene/Ru(0001) moiré overlayer. *J. Chem. Phys.* **131,** 164701 (2009).
38. Zhang, H. G. *et al.* Assembly of iron phthalocyanine and pentacene molecules on a graphene monolayer grown on Ru(0001). *Phys. Rev. B* **84,** 245436 (2011).
39. Yang, K. *et al.* Molecule–substrate coupling between metal phthalocyanines and epitaxial graphene grown on Ru(0001) and Pt(111). *J. Phys. Chem. C* **116,** 14052–14056 (2012).
40. Balog, R. *et al.* Bandgap opening in graphene induced by patterned hydrogen adsorption. *Nature Mater.* **9,** 315–319 (2010).
41. Rusponi, S. *et al.* Highly anisotropic Dirac cones in epitaxial graphene modulated by an island superlattice. *Phys. Rev. Lett.* **105,** 246803 (2010).
42. Scardamaglia, M. *et al.* Graphene-induced substrate decoupling and ideal doping of a self-assembled iron-phthalocyanine single layer. *J. Phys. Chem. C* **117,** 3019–3027 (2013).
43. Loginova, E., Nie, S., Thürmer, K., Bartelt, N. C. & McCarty, K. F. Defects of graphene on Ir(111): rotational domains and ridges. *Phys. Rev. B* **80,** 085430 (2009).
44. Vo-Van, C. *et al.* Epitaxial graphene prepared by chemical vapor deposition on single crystal thin iridium films on sapphire. *Appl. Phys. Lett.* **98,** 181903 (2011).
45. Hattab, H. *et al.* Growth temperature dependent graphene alignment on Ir(111). *Appl. Phys. Lett.* **98,** 141903 (2011).
46. Meng, L. *et al.* Multi-oriented moiré superstructures of graphene on Ir(111): experimental observations and theoretical models. *J. Phys. Condens. Matter* **24,** 314214 (2012).
47. Jean, F. *et al.* Effect of preparation on the commensurabilities and thermal expansion of graphene on Ir(111) between 10 and 1300 K. *Phys. Rev. B* **88,** 165406 (2013).
48. Hämäläinen, S. K. *et al.* Structure and local variations of the graphene moiré on Ir(111). *Phys. Rev. B* **88,** 201406(R) (2013).
49. Blanc, N. *et al.* Local deformations and incommensurability of high-quality epitaxial graphene on a weakly interacting transition metal. *Phys. Rev. B* **86,** 235439 (2012).
50. Hattab, H. *et al.* Interplay of wrinkles, strain, and lattice parameter in graphene on iridium. *Nano Lett.* **12,** 678–682 (2012).
51. Martoccia, D. *et al.* Graphene on Ru(0001): a 25 × 25 supercell. *Phys. Rev. Lett.* **101,** 126102 (2008).
52. Iannuzzi, M. *et al.* Moiré beatings in graphene on Ru(0001). *Phys. Rev. B* **88,** 125433 (2013).
53. Merino, P., Švec, M., Pinardi, A. L., Otero, G. & Martín-Gago, J. A. Strain-driven moiré superstructures of epitaxial graphene on transition metal surfaces. *ACS Nano* **5,** 5627–5634 (2011).
54. Sutter, P., Sadowski, J. T. & Sutter, E. Graphene on Pt(111): growth and substrate interaction. *Phys. Rev. B* **80,** 245411 (2009).
55. Lee, J.-U., Yoon, D. & Cheong, H. Estimation of Young's modulus of graphene by Raman spectroscopy. *Nano Lett.* **12,** 4444–4448 (2012).
56. Hermann, K. Periodic overlayers and moiré patterns: theoretical studies of geometric properties. *J. Phys. Condens. Matter* **24,** 314210 (2012).
57. Zeller, P. & Günther, S. What are the possible moiré patterns of graphene on hexagonally packed surfaces? *New J. Phys.* **16,** 083028 (2014).
58. Miniussi, E. *et al.* The competition for graphene formation on Re(0001): a complex interplay between carbon segregation, dissolution and carburisation. *Carbon* **73,** 389–402 (2014).
59. Miniussi, E. *et al.* Thermal stability of corrugated epitaxial graphene grown on Re(0001). *Phys. Rev. Lett.* **106,** 216101 (2011).
60. Marchini, S., Günther, S. & Wintterlin, J. Scanning tunneling microscopy of graphene on Ru(0001). *Phys. Rev. B* **76,** 075429 (2007).
61. Pan, Y. *et al.* Highly ordered, millimeter-scale, continuous, single-crystalline graphene monolayer formed on Ru(0001). *Adv. Mater.* **21,** 2777–2780 (2009).
62. Voloshina, E. N., Dedkov, Y. S., Torbrügge, S., Thissen, A. & Fonin, M. Graphene on Rh(111): Scanning tunneling and atomic force microscopies studies. *Appl. Phys. Lett.* **100,** 241606 (2012).
63. Nysten, B., Roux, J.-C., Flandrois, S., Daulan, C. & Saadaoui, H. AFM-STM studies of carbonization and graphitization of polyimide films. *Phys. Rev. B* **48,** 12527–12551 (1993).
64. Miyake, K. *et al.* Giant superstructures formed on graphite surface treated with NaOH solutions studied by scanning tunneling microscopy. *Ultramicroscopy* **73,** 185–189 (1998).
65. Osing, J. & Shvets, I. V. Bulk defects in graphite observed with a scanning tunneling microscope. *Surf. Sci.* **417,** 145–150 (1998).
66. Blanc, N., Jean, F., Krasheninnikov, A. V., Renaud, G. & Coraux, J. Strains induced by point defects in graphene on a metal. *Phys. Rev. Lett.* **111,** 085501 (2013).
67. Jean, F. *et al.* Topography of the graphene/Ir(111) moiré studied by surface x-ray diffraction. *Phys. Rev. B* **91,** 245424 (2015).
68. Carozo, V. *et al.* Raman signature of graphene superlattices. *Phys. Rev. B* **11,** 4527–4534 (2011).
69. Carozo, V. *et al.* Resonance effects on the Raman spectra of graphene superlattices. *Phys. Rev. B* **88,** 085401 (2013).

70. Cocco, G., Cadelano, E. & Colombo, L. Gap opening in graphene by shear strain. *Phys. Rev. B* **81,** 241412(R) (2010).
71. Nguyen, V. H. & Dollfus, P. Strain-induced modulation of Dirac cones and van Hove singularities in a twisted graphene bilayer. *2D Mater.* **2,** 035005 (2015).
72. Zeller, P., Dänhardt, S., Gsell, S., Schreck, M. & Wintterlin, J. Scalable synthesis of graphene on single crystal Ir(111) films. *Surf. Sci.* **606,** 1475–1480 (2012).
73. Natterer, F. D., Rusponi, S., Papagno, M., Carbone, C. & Brune, H. Optimizing long-range order, band gap, and group velocities for graphene on close-packed metal surfaces. *J. Phys. Condens. Matter* **24,** 314203 (2012).
74. Man, K. L. & Altman, M. S. Small-angle lattice rotations in graphene on Ru(0001). *Phys. Rev. B* **84,** 235415 (2011).
75. Hass, J. *et al.* Why multilayer graphene on 4H-SiC(000$\bar{1}$) behaves like a single sheet of graphene. *Phys. Rev. Lett.* **100,** 125504 (2008).
76. Varchon, F., Mallet, P., Magaud, L. & Veuillen, J.-Y. Rotational disorder in few-layer graphene films on 6H-SiC(000-1): A scanning tunneling microscopy study. *Phys. Rev. B* **77,** 165415 (2008).
77. Emtsev, K. V. *et al.* Towards wafer-size graphene layers by atmospheric pressure graphitization of silicon carbide. *Nature Mater.* **8,** 203–207 (2009).
78. Kresse, G. & Hafner, J. Ab initio molecular dynamics for liquid metals. *Phys. Rev. B* **47,** 558–561 (1993).
79. Kresse, G. & Joubert, D. From ultrasoft pseudopotentials to the projector augmented-wave method. *Phys. Rev. B* **59,** 1758 (1999).
80. Perdrew, J. P., Burke, K. & Ernzerhof, M. General gradient approximation made simple. *Phys. Rev. Lett.* **77,** 3865–3868 (1996).

Acknowledgements

Financial support from Agence Nationale de la Recherche through contract ANR-14-OHRI-0004-01 2DTransformers is acknowledged. Calculations were performed using HPC resources from GENCI-IDRIS (Grant 2015-097015). We thank Jean-Yves Veuillen and Karim Ferhat for fruitful discussions. T.L.Q. was supported by a CIBLE fellowship from Région Rhône-Alpes.

Author Contributions

C.C. and J.C. conceived the experiments, A.A., T.L.Q., V.G. and P.D. conducted the experiments, L.M. performed the simulations, A.A. analysed the results. All authors reviewed the manuscript.

Additional Information

Supplementary information accompanies this paper at http://www.nature.com/srep

Competing financial interests: The authors declare no competing financial interests.

How to cite this article: Artaud, A. *et al.* Universal classification of twisted, strained and sheared graphene moiré superlattices. *Sci. Rep.* **6**, 25670; doi: 10.1038/srep25670 (2016).